Available online at www.sciencedirect.com
ScienceDirect
Trans. Nonferrous Met. Soc. China 32(2022) 1290−1300
Transactions of Nonferrous Metals Society of China
www.tnmsc.cn

φ−pH diagrams and kinetics of V_2O_3 prepared by solution-phase hydrogen reduction

Yi-bo HU[1,2,3,4], Yi-min ZHANG[1,2,3,4], Nan-nan XUE[1,2,3,4], Peng-cheng HU[1,2,3,4], Liu-hong ZHANG[1,2,3,4]

1. College of Resources and Environmental Engineering, Wuhan University of Science and Technology, Wuhan 430081, China;
2. State Environmental Protection Key Laboratory of Mineral Metallurgical Resources Utilization and Pollution Control, Wuhan University of Science and Technology, Wuhan 430081, China;
3. Hubei Collaborative Innovation Center for High Efficient Utilization of Vanadium Resources, Wuhan 430081, China;
4. Hubei Provincial Engineering Technology Research Center of High Efficient Cleaning Utilization for Shale Vanadium Resource, Wuhan University of Science and Technology, Wuhan 430081, China

Received 25 March 2021; accepted 26 September 2021

Abstract: Solution-phase hydrogen reduction (SpHR) was introduced into V_2O_3 preparation to overcome disadvantages of traditional reduction roasting, which include a long process, high energy consumption, and generation of pollution. The research mainly focuses on φ−pH diagrams and kinetics of SpHR. Thermodynamic analysis of φ−pH diagrams for the V−H_2O system demonstrates that V_2O_3 preparation via SpHR requires a high temperature, a high vanadium concentration, and sufficient hydrogen in acidic solution. Kinetic analyses show that the activation energy of V_2O_3 preparation via SpHR is 38.0679 kJ/mol, indicating that the reduction is controlled by a combination of interfacial chemical reaction and internal diffusion. Effects of H_2 partial pressure (slope K=0.05246) on the reaction rate is not as significant as the vanadium concentration (K=1.58872). V_2O_3 crystals with a purity of 99.59% and a vanadium precipitation rate of 99.83% were obtained under the following conditions: pH=5−6, c(V_2O_5)=0.5 mol/L, p(H_2)=4 MPa, m($PdCl_2$)=10 mg, T=250 °C, and t=2.5 h.

Key words: V_2O_3; solution-phase hydrogen reduction; φ−pH diagram; kinetics

1 Introduction

V_2O_3 is a vanadium oxide that has a high melting point and is reducible. It can be prepared directly from vanadium powder, ferrovanadium alloy, vanadium carbide, vanadium nitride, and other products [1,2]. Because the phase transition, magnetic susceptibility, optical transmittance, and reflectivity of V_2O_3 change with temperature, it also has important applications in thermoelectric switches, magnetic switches, optical switches, and film materials [3,4].

In China, research on the preparation of V_2O_3 began in the 1960s [5]. Generally, vanadium pentoxide, ammonium metavanadate, and polyvanadate have been used to prepare V_2O_3 via reduction roasting [6]. Traditional research methods require the preparation of precursors (which lengthen the production process) and also increase the energy consumption of roasting [7].

Solution-phase hydrogen reduction (SpHR) is an efficient way to prepare metallic powders because SpHR consumes less energy, has high productivity, and is eco-friendly and economically feasible [8]. Furthermore, it is possible to control the properties of the product through the use of a catalyzer and surface-active agents and by adjusting

Corresponding author: Yi-min ZHANG, E-mail: zym126135@126.com
DOI: 10.1016/S1003-6326(22)65874-6

the autoclave conditions [9]. XU et al [10] used SpHR of sodium tungstate, citric acid, and sodium sulfate in an autoclave to fabricate WO_3 precursor powders with nanorods; then, they used H_2 to reduce the precursor to obtain ultrafine La_2O_3-doped tungsten powders. AGRAWAL et al [11] reviewed the production of nickel and copper powders from solutions using SpHR under pressure, and the composite materials of required specifications were produced using coating nickel or copper powders on secondary materials such as graphite, tungsten carbide, and aluminum [11]. LIANG et al [12] obtained metallic silver from a Ag_2S alkaline slurry using $PdCl_2$ as a catalyst at 220 °C, pH=12.0, and 2−3 MPa of partial H_2 pressure for 4 h; the Ag transformation from Ag_2S can reach 95% using SpHR.

On the basis of the above, SpHR is widely used in metal precipitation, but few studies on vanadium precipitation have been reported. Our previous study [13] indicated that vanadium cannot be precipitated directly from solution, and the lowest valence that can be prepared using SpHR is V_2O_3. But until now, there has been a lack of research on the thermodynamics and kinetics of the system.

In this work, the thermodynamics and kinetics of the preparation of V_2O_3 via SpHR were investigated. Thermodynamics study focuses on the φ−pH diagram of the V−H_2O system, and a set of φ−pH diagrams at elevated temperatures, different vanadium concentrations, and H_2 partial pressure were constructed to provide guidance on SpHR. A detailed study of the kinetic effects of temperature, vanadium concentration, and H_2 partial pressure for the process of preparing V_2O_3 via SpHR was carried out, and the kinetics mechanism was structured simply.

2 Research methods

2.1 Electrode potential and pH value

The redox reaction in solution can be shown as follows [14]:

$$aP_b+nH^++ze=bQ_a+n/2H_2O \quad (1)$$

where P_b and Q_a are defined as the particular vanadium species, a and b are the number of V atoms in species, n is the number of H^+, and z is the number of electrons obtained.

According to the Nernst equation, the relationship between the pH of a solution and the electrode potential (φ) can be expressed as [15]:

$$\varphi=\varphi^{\Theta}-\frac{RT}{zF}\ln\left(\frac{\alpha_{\mathrm{Q}}^{b}}{\alpha_{\mathrm{P}}^{a}\alpha_{\mathrm{H}^+}^{n}}\right) \quad (2)$$

where R is the molar gas constant, T is the thermodynamic temperature, F is the Faraday constant (96485 C/mol), φ^{Θ} is the standard electrode potential, and α is the ionic activities of species P_b, Q_a, and H^+.

If the activities of P_b and Q_a are regarded as their molar concentrations $c_{V(\mathrm{P})}$ and $c_{V(\mathrm{Q})}$, they follow that [16],

$$c_{V(\mathrm{P})}=c_{V(\mathrm{Q})}=\frac{\sum c_V}{2} \quad (3)$$

$$c_{V(\mathrm{P})}=bc_{\mathrm{P}},\ c_{V(\mathrm{Q})}=ac_{\mathrm{Q}} \quad (4)$$

$$\varphi^{\Theta}=\frac{-\Delta_{\mathrm{r}}G_{\mathrm{m}}^{\Theta}}{zF} \quad (5)$$

According to Eqs. (4) and (5), the Nernst equation can be written as Eq. (6):

$$\varphi=-\frac{\Delta_{\mathrm{r}}G_{\mathrm{m}}^{\Theta}}{zF}-\frac{2.303RT}{zF}\lg\frac{(c_{V(\mathrm{Q})}/a)^b}{(c_{V(\mathrm{P})}/b)^a}-\frac{2.303RT}{zF}n\mathrm{pH} \quad (6)$$

The procedures require drawing an φ−pH diagram, as shown in Eq. (6). First, it is necessary to know that the vanadium species and the reactions that may exist in solution in the system. Then, thermodynamic data from Refs. [17,18], e.g. the standard Gibbs free-energy of formation ($\Delta_{\mathrm{f}}G_{\mathrm{m}}^{\Theta}$), should be consulted. For general chemical reactions: $aA+bB\rightarrow cC+dD$, the standard Gibbs free-energy of reaction ($\Delta_{\mathrm{r}}G_{\mathrm{m}}^{\Theta}$) is obtained using $\Delta_{\mathrm{r}}G_{\mathrm{m}}^{\Theta}=c\Delta_{\mathrm{f}}G_{\mathrm{C}}^{\Theta}+d\Delta_{\mathrm{f}}G_{\mathrm{D}}^{\Theta}-(a\Delta_{\mathrm{f}}G_{\mathrm{A}}^{\Theta}+b\Delta_{\mathrm{f}}G_{\mathrm{B}}^{\Theta})$. Finally, the relationship between pH and species concentration is calculated using the data and reactions (Appendix: Tables 1 and 2).

2.2 Reaction rate and activation energy

First, the V_2O_5 solution was completely dissolved in NaOH solution, and the pH was adjusted to a certain value using H_2SO_4 solution, which was used as a feed solution. Second, the feed solution and $PdCl_2$ powder were placed in an autoclave (MCT 250, SenLong Co., Ltd., Beijing,

China). After the autoclave was flushed with N_2, it was gradually heated to a predetermined temperature. Third, a certain partial pressure of H_2 was introduced into the autoclave and maintained for 2 h for the reaction at a predetermined temperature and with a stirring speed of 300 r/min. During this time, samples were taken at intervals, and the vanadium concentration was measured. Fourth, after cooling and releasing the pressure, a slurry containing V_2O_3 was collected from the autoclave, and the slurry was filtered and vacuum dried to obtain V_2O_3 products.

In SpHR, the precipitation rate of vanadium (λ) was calculated using the following equation:

$$\lambda=\left(1-\frac{c_2V_2}{c_1V_1}\right)\times100\% \tag{7}$$

where c_1 and c_2 are the vanadium concentrations in the feed solution and precipitated liquid, respectively; V_1 and V_2 are the volumes of feeding solution and precipitated liquid, respectively.

The differential method was used in the kinetics of V_2O_3 preparation via SpHR. When the curve of vanadium concentration is drawn with respect to reaction time for the experiment, the tangent of the curve can be obtained at a specified time, and the rate equation of reaction can be written as follows [19]:

$$r_i=-\frac{\mathrm{d[M]}}{\mathrm{d}t_i} \tag{8}$$

where r_i is the rate of the reaction at t_i, t is the reaction time, and [M] is the concentration of vanadium.

The rate of the reaction (r_i) and the concentration of vanadium ([M]) conform to the following relationship:

$$\ln r_i=\ln k+m\ln[\mathrm{M}] \tag{9}$$

where k is the rate constant of the reaction, and m is the reaction order.

It is known that $\ln r_i$ changes in a slope line with ln[M], and the intercept is $\ln k$. According to the Arrhenius equation, A is a constant, there is a linear relationship between $\ln k$ and $1/T$, and the slope (β) is $-E_a/R$ [20]:

$$\ln k=-\frac{E_a}{RT}+A=-\beta\frac{1}{T}+A \tag{10}$$

where E_a is the the activation energy.

3 Results and discussion

3.1 φ−pH diagrams of V_2O_3 preparation via SpHR

φ−pH diagrams, which are also known as Pourbaix diagrams, show the predominant thermodynamic areas of different species in solution. This is a common, intuitive thermodynamic tool in the field of vanadium extraction [14,21]. However, little systematic research has focused on the factors that affect a φ−pH diagram. Inspired by this, a set of φ−pH diagrams for V−H_2O system at elevated temperatures, different vanadium concentrations, and H_2 partial pressure were constructed to provide guidance for V_2O_3 preparation via SpHR.

3.1.1 Vanadium species in solution

The complexity and diversity of vanadium species depend greatly on the concentration of vanadium, and this makes research using φ−pH diagrams of the V−H_2O system difficult [22]. Thus, it is important that the lg c−pH equilibrium equations are calculated using Eq. (6), and this is used to determine the vanadium species and to lay a foundation for the φ−pH diagram. The lg c−pH diagrams of V(II)−V(V) at 25 °C are shown in Fig. 1.

As seen in Fig. 1, vanadium species mainly exist in a mononuclear form at a low concentration, and polynuclear vanadate may be dominant in certain areas at a high concentration. Furthermore, as seen in Figs. 1(c) and (d), a high valence (i.e., V(IV) and V(V)) tends to produce polynuclear vanadate more easily at a high concentration ($\geq10^{-2}$ mol/L) and high pH, and these are common conditions in practice [23].

3.1.2 φ−pH diagram of V−H_2O system at elevated temperatures

According to Ref. [24] and data from Factsage, the effect of elevated temperature (25−300 °C) on the φ−pH diagram of the V−H_2O system was studied at a vanadium concentration of 1 mol/L and H_2 partial pressure of 0 MPa; the results are shown in Fig. 2. It must be explained that vanadium species, especially polynuclear vanadate, have incomplete thermodynamic data at elevated temperatures. This leads to a slight simplification of the φ−pH diagram of the V−H_2O system, and the simplified lines are replaced by ellipsis (⋯), such

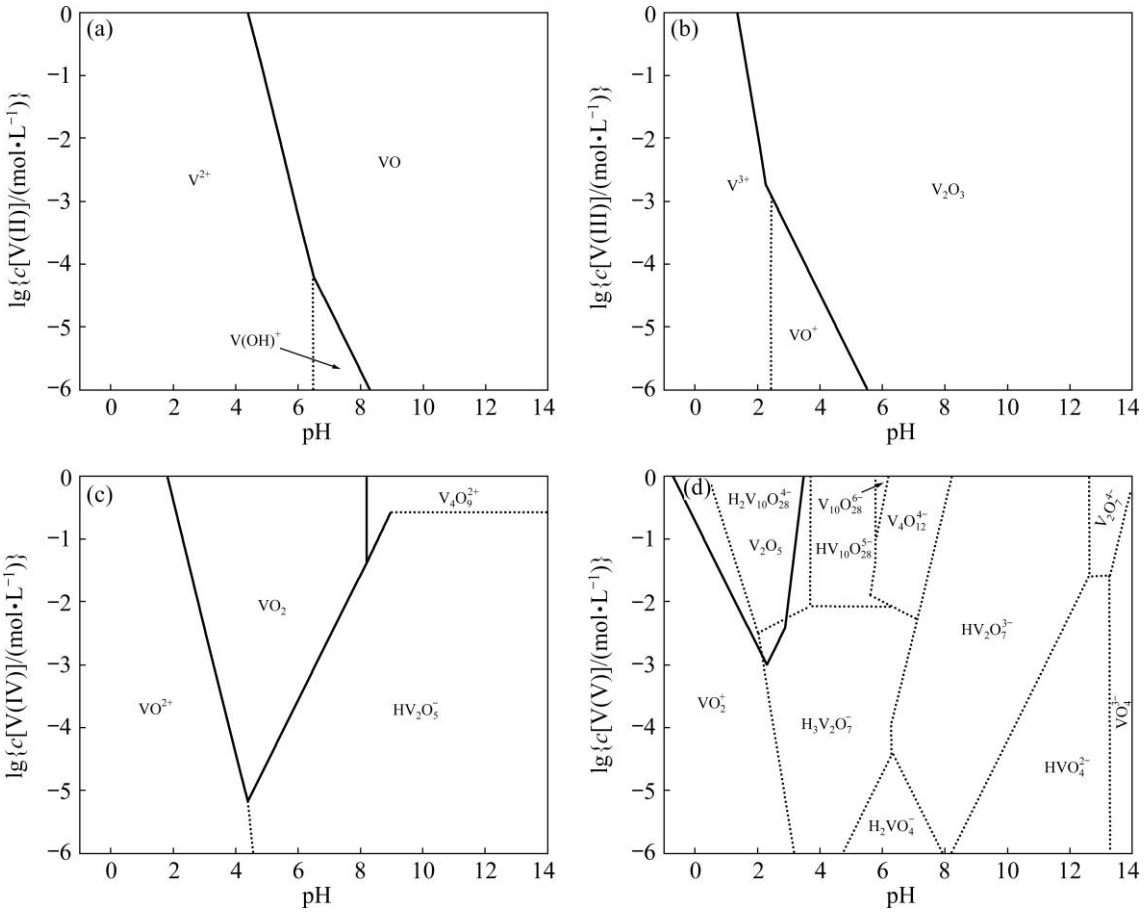

Fig. 1 lg c−pH diagrams of V(II) (a), V(III) (b), V(IV) (c), and V(V) (d) (Dotted lines: equilibrium between two ionic species; Solid lines: equilibrium between oxides and ionic species) (Appendix: Table 1)

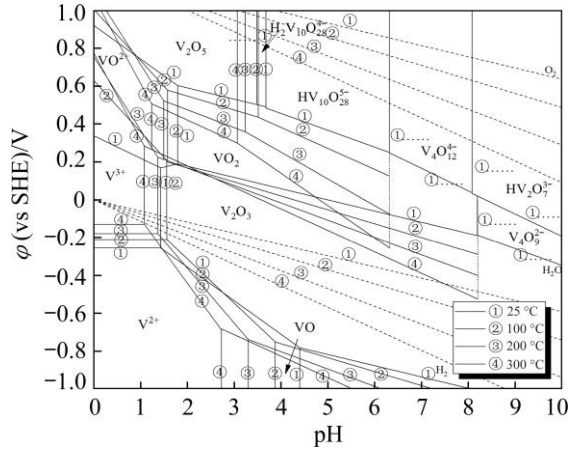

Fig. 2 φ−pH diagram of V−H_2O system at elevated temperatures (Dotted lines: stability area of H_2O; Solid lines: equilibrium of different vanadium species) (Appendix: Tables 2 and 3)

as the lines of $HV_{10}O_{28}^{5-}/V_4O_{12}^{4-}$ at 100, 200, and 300 °C.

The φ−pH diagram of the V−H_2O system shows that the predominant area of V_2O_3 occupies a large area. This indicates that V_2O_3 is a stable and easily obtained product at a suitable potential and concentration of vanadium. Also, the hydrogen lines are lower than the potential of high valence vanadium reduction to V(III), and this demonstrates that V_2O_3 can be prepared via solution-phase reduction in thermodynamics.

As seen in Fig. 2, elevated temperatures cause the equilibrium line of vanadium oxide dissolution to move to the region with lower pH because of the change in $\Delta_f G_m^{\Theta}$. This increases the predominant area of V_2O_3. According to Eq. (6), the slope of a diagonal line in the φ−pH diagram (a reaction that involves both electrons and H^+) is proportional to the temperature; that is, the elevated temperature increases the slope. It should be noted that the slope of the hydrogen line is steeper than the high-valence vanadium reduction to V(III), and this also increases the area of V_2O_3.

As discussed above, when the temperature increases, movement of the equilibrium line and an increase in the slope extend the area of V_2O_3 above the hydrogen line. This is beneficial to preparation

via SpHR. In addition, the reaction from ion to oxide is endothermic, and thus, elevated temperature has a favorable effect on the preparation of V_2O_3.

3.1.3 φ–pH diagram of V−H_2O system at different vanadium concentrations

According to Eq. (3), changes in vanadium concentration affect the concentration of dissolved species, and this causes the equilibrium lines in the φ–pH diagram to move. The effect of vanadium concentration (10^{-2}–10^{1} mol/L) on the φ–pH diagram of the V−H_2O system was studied at a temperature of 25 °C and H_2 partial pressure of 0 MPa, as shown in Fig. 3. It must be explained from Fig. 1 that V(IV) species change with respect to concentration, and this cannot be reflected in one diagram; thus, simplified lines are replaced by ellipsis (⋯).

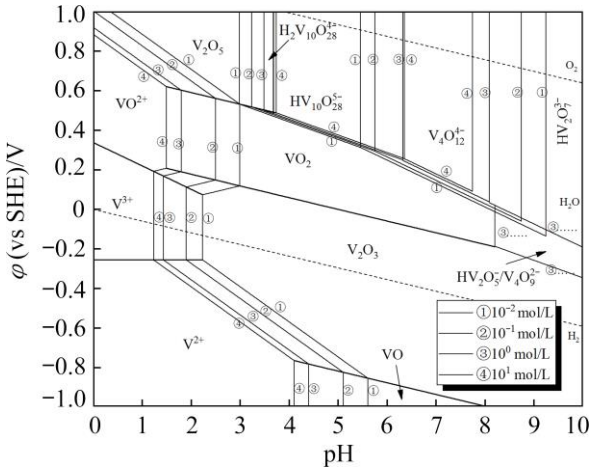

Fig. 3 φ–pH diagram of V−H_2O system at different vanadium concentrations (Appendix: Table 4)

As seen from Fig. 3, an increase in the vanadium concentration results in the equilibrium lines of V^{3+}/V_2O_3, V^{2+}/V_2O_3, and VO^{2+}/V_2O_3, moving to the region with low pH. This expands the area of V_2O_3. This phenomenon also occurs in the predominant areas of other vanadium oxides. Some lines do not change with respect to the vanadium concentration. The equilibrium lines of V_2O_3/VO and V_2O_3/VO_2 do not move with the change of vanadium concentration because there are no ions involved between vanadium oxides. Also, since $\lg[(c_{V(Q)}/a)^b]/[(c_{V(P)}/b)^a]$ is offset during the calculation, the concentration of ions with the same number of vanadium atoms does not affect the equilibrium line.

In practice, the concentration of vanadium decreases with the preparation process. This indicates that the predominant area of V_2O_3 is smaller, and the preparation tendency will be reduced, especially at the end of preparation. Thus, it is necessary to ensure the concentration of vanadium in V_2O_3 preparation via SpHR.

3.1.4 φ–pH diagram of V−H_2O system at different H_2 partial pressures

In the V−H_2O system, H_2 partial pressure only affects the placement of the hydrogen line in the φ–pH diagram. The electrode reaction of H_2O and the relationship of φ–pH are as follows [25]:

Potential reaction: $O_2+4H^++4e=2H_2O$ (11)

Cathode reaction: $4H^++4e=2H_2$ (12)

$$\varphi_{(H_2/H^+)}=\varphi^{\Theta}_{(H_2/H^+)}+\frac{2.303RT}{zF}\lg p(H_2)+\frac{9.212RT}{zF}\mathrm{pH} \quad (13)$$

where $\varphi^{\Theta}_{(H_2/H^+)}$ is the standard electrode potential of hydrogen (0 V).

The effect of H_2 partial pressure (0−6 MPa) on the φ–pH diagram of the V−H_2O system was studied at a temperature of 25 °C and vanadium concentration of 1 mol/L, and the results are shown in Fig. 4.

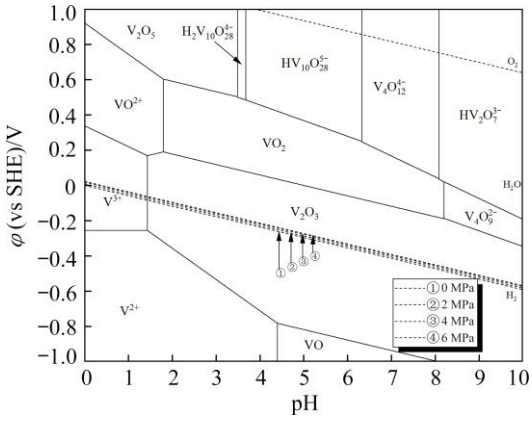

Fig. 4 φ–pH diagram of V−H_2O system at different H_2 partial pressures (Appendix: Table 5)

Figure 4 shows that the H_2 partial pressure has little effect on the φ–pH diagram. The high partial pressure of hydrogen causes the hydrogen line to move up. Although it decreases the predominant area of V_2O_3 in solution-phase, sufficient hydrogen will make the V−H_2O system at a lower potential, and this ensures that a reducing atmosphere is used in the preparation of V_2O_3.

Figures 2−4 show that when the pH is higher, the electrode potential is lower. This suggests that an increase in pH leads to a decreased possibility of preparing V_2O_3 in a fixed system. Furthermore, a lower pH is beneficial for the preparation of V_2O_3, according to Eq. (6). In summary, preparing V_2O_3 via SpHR requires high temperature, high vanadium concentration, and sufficient hydrogen in acidic solution.

3.2 Kinetics of V_2O_3 preparation via SpHR

The obtained results in the thermodynamic analysis show that temperature, vanadium concentration, and H_2 partial pressure affect the possibility of preparing V_2O_3 via SpHR.

φ−pH diagrams for the V−H_2O system illustrate the conditions and trends via SpHR to prepare V_2O_3, but they do not reflect the reaction state of the process. A three-phase reaction system of gas, solution, and solid has a complicated structure for the V_2O_3 preparation via SpHR, and thus, the kinetics process of the reaction in the system needs to be illustrated. Therefore, the effects of temperature, vanadium concentration, and H_2 partial pressure on the kinetics of V_2O_3 preparation were first investigated.

3.2.1 Effects of temperature

The results are presented in terms of the concentration of vanadium that remained in solution with respect to the reaction time. Figure 5 shows the effects of the temperature when the vanadium concentration was 0.3 mol/L and the H_2 partial pressure was 4 MPa. The effects of temperature on the precipitation rate and XRD patterns (D/MAX-RB X-ray Diffractometer, Rigaku, Tokyo, Japan) of the products are shown in Fig. 6. Meanwhile, a trace of $PdCl_2$ was used as an effective catalyst to improve the H_2 activity [12].

It can be concluded from Fig. 5 that increasing temperature increases the rate of reaction and promotes the reaction to be more complete. In a early period, the solution reaction mainly focused on improving the reduction activity of H_2, as shown in Fig. 6(a), and the period decreased or even disappeared with an increase in temperature. According to Fig. 5(a) and Eqs. (9) and (10), the fitting line was obtained using the Arrhenius equation, and the results are shown in Fig. 5(b). The correlation coefficient (R^2) of the fitting line is 0.95435. Equation (10) can be used to calculate the activation energy (E_a) of the preparation of V_2O_3 via SpHR, and the value is 38.0679 kJ/mol; this indicates that the controlling step in the reduction is a mixed control [26].

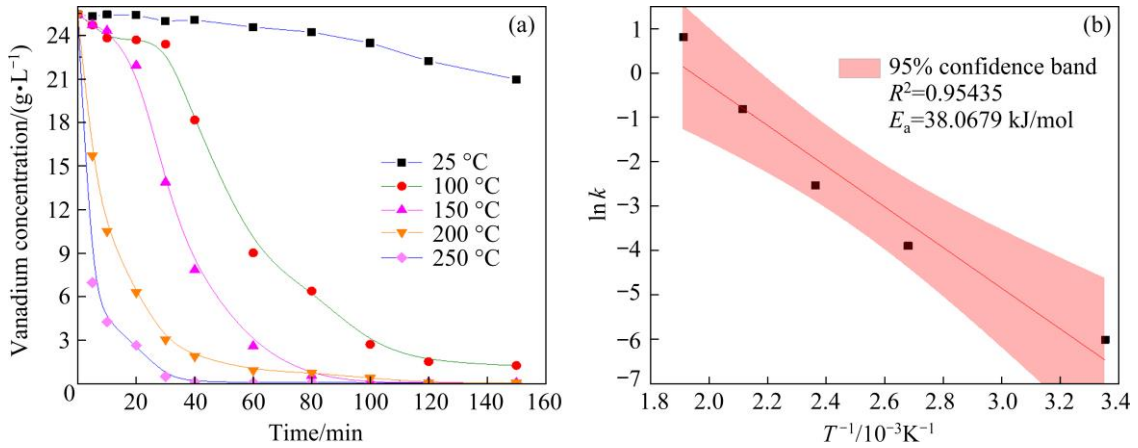

Fig. 5 Effects of temperature on kinetics of V_2O_3 preparation (a), and fitting line obtained using Arrhenius equation (b)

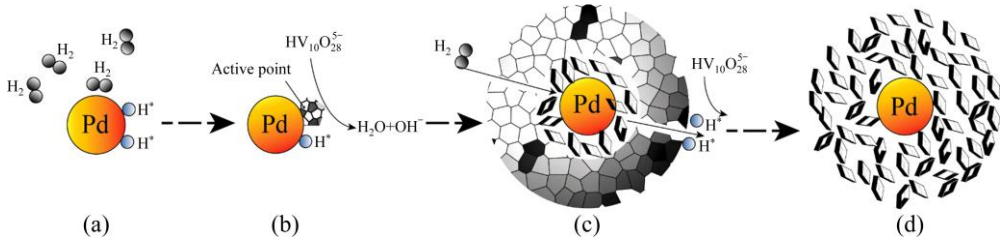

Fig. 6 Kinetics mechanism of preparation of V_2O_3 via SpHR: (a) H_2 activation; (b) Vanadium crystallization in solution at active point; (c) Internal diffusion control step; (d) V_2O_3 crystallization

ZHANG et al [13] summarized the phase transformation mechanism, that is, the vanadium in solution is first precipitated as V(IV) and then transformed into V_2O_3 with activated hydrogen. Inspired by this, it can be speculated that the preparation of V_2O_3 via SpHR may follow two steps: (1) In the earlier time (Fig. 6(b)), a relatively high concentration of vanadium in the solution ensures that the reaction interface has a strong chemical driving force and forms V(IV) crystals; thus, the reduction is controlled by an interfacial chemical reaction. (2) With a gradual decrease in the vanadium concentration, the mass transfer rate also slows, and the reduction is controlled by the internal diffusion of activated hydrogen inside the crystal (Fig. 6(c)).

Figure 7 shows that temperature has a significant effect on the precipitation rate and the phase of vanadium. According to Fig. 7(a), the precipitation rate increases from 5.6% to 99.83% as the temperature increases from 25 to 250 °C. Also, there is no obvious change in the precipitation rate with a further increase in the temperature to 250 °C. However, Fig. 7(b) shows that the diffraction peaks of the product that was obtained at 200 °C do not appear as a phase of V_2O_3, and have an inconspicuous crystal. To explore the phase transformation of a product, an XRD pattern was recorded at 240 °C. According to patters (4) and (5) in Fig. 7(b), the diffraction peaks of V_2O_3 can be observed at 240 °C. However, the crystals are still indistinct, and pure V_2O_3 crystals are obtained when the temperature reaches 250 °C. This implies that the phase of the product changes between 240 and 250 °C. In practice, the temperature should be higher than 250 °C to ensure that the energy is high enough for the preparation of V_2O_3.

3.2.2 Effects of vanadium concentration

Figure 8 shows the effects of vanadium concentration on the time when the temperature was 250 °C and the H_2 partial pressure was 4 MPa. The effects of vanadium concentration on the precipitation rate and XRD patterns of the products are shown in Fig. 9.

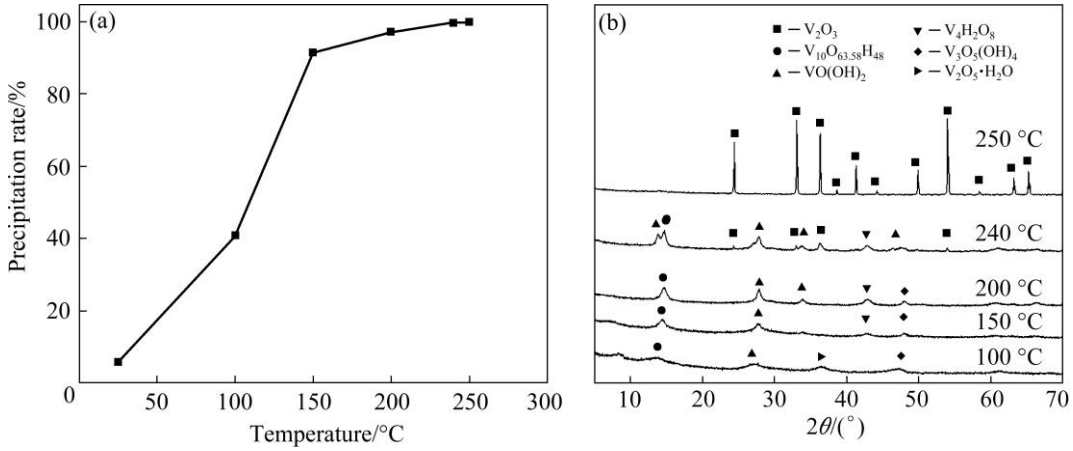

Fig. 7 Effects of temperature on precipitation rate (a), and XRD patterns of products at different temperatures (b)

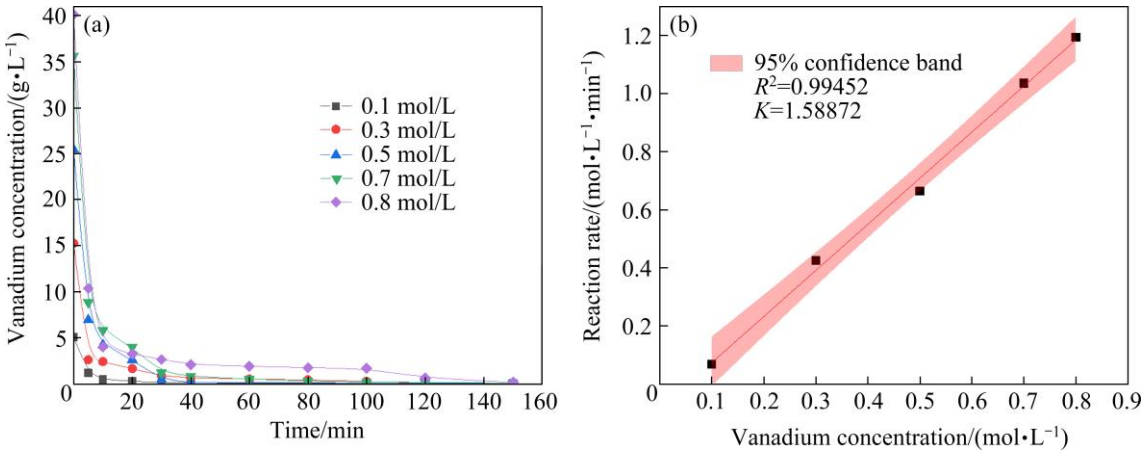

Fig. 8 Effects of vanadium concentration on kinetics of V_2O_3 preparation (a) and fitting line of reaction rate (b)

As seen in Fig. 8, a high vanadium concentration results in a higher reaction rate because the concentration affects the ability of mass transfer in solution. For example, the reaction rate reaches 1.194 mol/(L·min) at 0.8 mol/L, but it only reaches 0.4252 mol/(L·min) at a vanadium concentration of 0.1 mol/L. The fitting line of reaction rate indicates that the slope (K) reaches 1.58872, and the correlation coefficient (R^2) of the fitting line is 0.99452. The residual vanadium in solution varies within 30 min at 0.1−0.8 mol/L, but the residual vanadium basically remains at the same level with a further increase in time.

Figure 9 shows that the effect of vanadium concentration on the precipitation rate and phase of vanadium. According to Fig. 9(a), the precipitation rate increases from 98.29% to 99.83% with an increase in the concentration from 0.1 to 0.5 mol/L, and the precipitation rate at concentrations of 0.7 and 0.8 mol/L decreases slightly because of insufficient H_2 partial pressure. The XRD patterns for the products are presented in Fig. 9(b). Pure diffraction peaks of V_2O_3 crystals can be observed when the vanadium concentration is higher than 0.3 mol/L. In contrast, the diffraction peaks are mixed phases of VOOH, $V_4H_2O_8$, and V_2O_3 when the vanadium concentration ranges from 0.1 to 0.3 mol/L. Moreover, Fig. 9(b) shows that the diffraction peak of V_2O_3 at 0.5 mol/L is the highest, and the diffraction peaks at 0.7 and 0.8 mol/L become gradually weaker, which is consistent with Fig. 9(a).

3.2.3 Effects of H_2 partial pressure

Figure 10 shows the effects of H_2 partial pressure when the temperature is 250 °C and the vanadium concentration is 0.5 mol/L. The effects of H_2 partial pressure on the precipitation rate and the XRD patterns of the products are shown in Fig. 11.

In Fig. 10(a), the reaction rate increases from 0.2773 to 0.5133 mol/(L·min) with an increase in the H_2 partial pressure from 0 to 4 MPa. The fitting line of the reaction rate indicates that the slope (K)

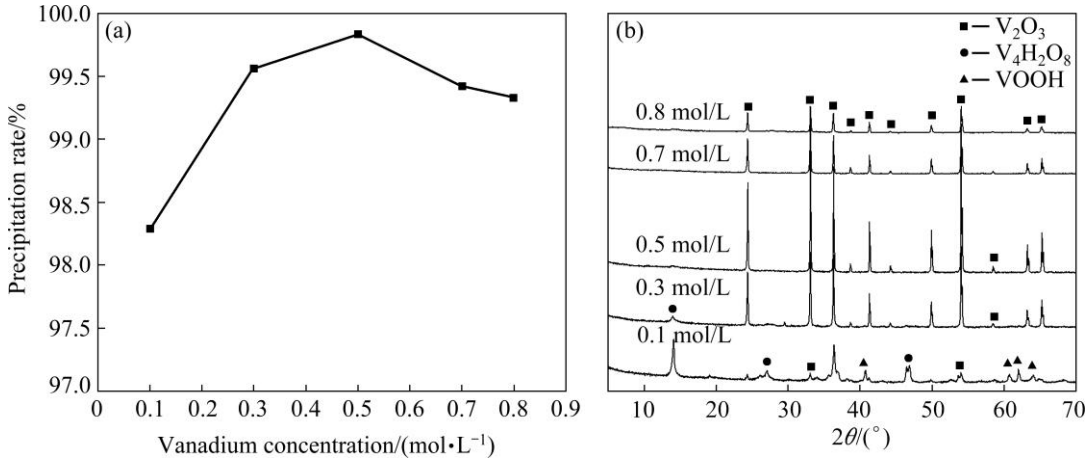

Fig. 9 Effects of vanadium concentration on precipitation rate (a), and XRD patterns of products at different vanadium concentrations (b)

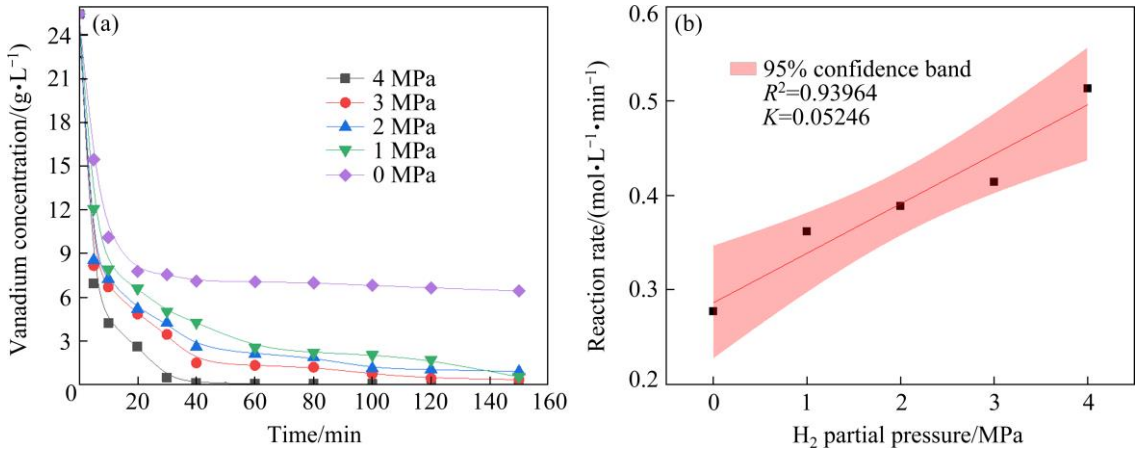

Fig. 10 Effects of H_2 partial pressure on kinetics of V_2O_3 preparation (a) and fitting line of reaction rate (b)

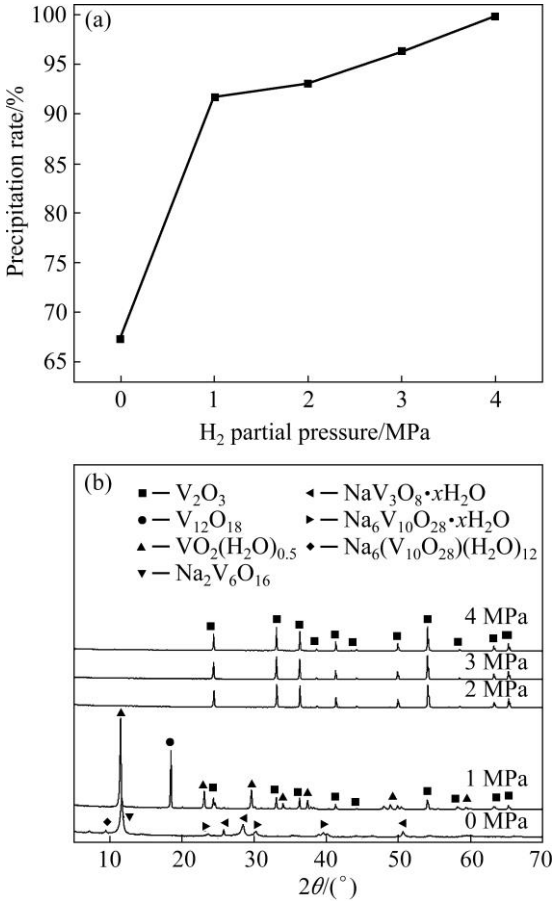

Fig. 11 Effects of H_2 partial pressure on precipitation rate (a), and XRD patterns of products at different H_2 partial pressures (b)

reaches 0.05246 with an R^2 value of 0.93964; this reveals that the effect of H_2 partial pressure on the reaction rate is not as significant as the vanadium concentration.

As seen in Fig. 11, H_2 partial pressure has a significant effect on the precipitation rate and phase of vanadium. The precipitation rate increases from 67.28% to 99.83% with an increase in the H_2 partial pressure from 0 to 4 MPa, and a higher H_2 partial pressure will be wasteful and expensive. When there is no H_2 in the solution (0 MPa), the diffraction peaks in the XRD pattern do not exhibit a reduction phase, but there are mixed diffraction peaks of V(V) crystals, such as $Na_6V_{10}O_{28} \cdot xH_2O$, $(Na_6V_{10}O_{28})(H_2O)_{12}$, $NaV_3O_8 \cdot xH_2O$, and $Na_2V_6O_{16}$. The diffraction peaks of V_2O_3 were observed when the H_2 partial pressure reached 1 MPa, but they were also mixed with the diffraction peaks of $VO_2(H_2O)_{0.5}$ and $V_{12}O_{18}$. For V_2O_3 crystals with a purity of 99.59%, a vanadium precipitation rate of 99.83% was obtained when the H_2 partial pressure was 4 MPa. Thus, it can be concluded that more hydrogen has no effect on the products.

To observe the morphology of the product, SEM (scanning electron microscopy, Carl Zeiss AG, Oberkochen, Germany) images and EDS (energy dispersive spectrometry, Oxford Instruments, Oxford, UK) analysis of the products are shown in Fig. 12 under the following conditions: pH of 5−6, $c(V_2O_5)$ of 0.5 mol/L, $p(H_2)$ of 4 MPa, $m(PdCl_2)$ of 10 mg, T of 250 °C, and t of 2.5 h. As seen in Fig. 12, most of the products are V_2O_3 crystals that are similar to a rhombohedral lattice [27], EDS analysis includes the vanadium/oxygen content of the point in Fig. 12, and it is very close to the mass fraction of V_2O_3.

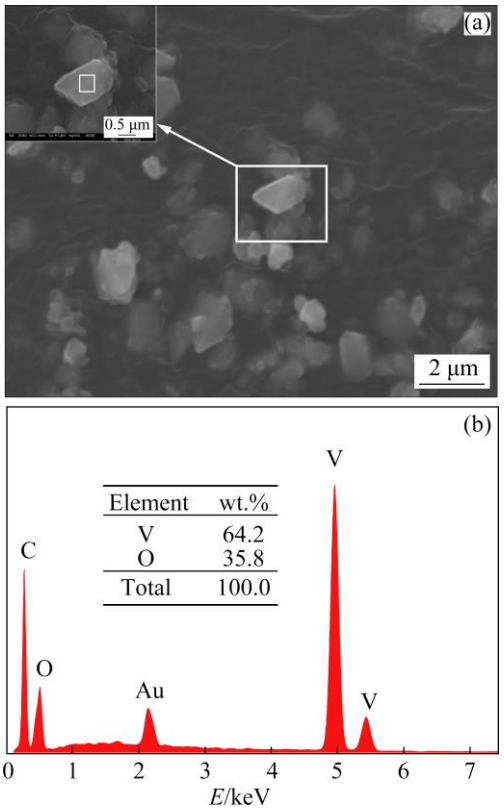

Fig. 12 SEM image (a) and energy dispersive spectrometer analysis (b) of vanadium products

4 Conclusions

(1) According to the thermodynamics analysis of V−H_2O system using φ−pH diagrams, an increase in the temperature and vanadium concentration extends the area of V_2O_3 above the hydrogen line. This is beneficial to the preparation via SpHR. H_2 partial pressure has little effect on the φ−pH diagram, but sufficient hydrogen will cause

the V−H_2O system to be at a lower potential. This can ensure that the preparation of V_2O_3 takes place in a reducing atmosphere.

(2) The activation energy of preparation of the V_2O_3 via SpHR is 38.0679 kJ/mol. This indicates that the reduction is controlled by a combination of interfacial chemical reaction and internal diffusion steps. The reduction is controlled by interfacial chemical reaction in the earlier time, and it is controlled by internal diffusion in the later time. The effects of vanadium concentration and H_2 partial pressure on the kinetics indicate that the effect of the H_2 partial pressure (K=0.05246) on the reaction rate is not as significant as the vanadium concentration (K=1.58872).

(3) V_2O_3 crystals with a purity of 99.59% and a vanadium precipitation rate of 99.83% were obtained under the following conditions: pH of 5−6, c(V_2O_5) of 0.5 mol/L, p(H_2) of 4 MPa, m($PdCl_2$) of 10 mg, T of 250 °C, and t of 2.5 h.

Acknowledgments

This work was financially supported by the National Key R&D Program of China (No. 2020YFC1909700), Outstanding Young and Middle-aged Science and Technology Innovation Team Project of Hubei Province, China (No. T201802), and the National Natural Science Foundation of China (No. 52004187).

Appendix

Appendix in this paper can be found at: http://www.ysxbcn.com/download/20-TNMSC-2021-0296-appendix.pdf.

References

[1] WANG Feng-kang, XU Bao-qiang, WAN He-li, YANG Jia, YANG Bin, JIANG Wen-long. Preparation of vanadium powders by calcium vapor reduction of V_2O_3 under vacuum [J]. Vacuum, 2020, 173: 109133.

[2] CHIRANJIVI L. Electronic, thermoelectric and optical properties of vanadium oxides: VO_2, V_2O_3 and V_2O_5 [D]. New Jersey: New Jersey Institute of Technology, 2015.

[3] SCHNEIDER K. Optical properties and electronic structure of V_2O_5, V_2O_3 and VO_2 [J]. Journal of Materials Science: Materials in Electronics, 2020, 31(13): 10478−10488.

[4] CHALOTRA S, MIR R A, KAUR G, PANDEY O P. Oxygen deficient V_2O_3: A stable and efficient electrocatalyst for HER and high performance EDLCs [J]. Ceramics International, 2020, 46(1): 703−714.

[5] BAI Yun-yu, JIN Ping, JI Shi-dong, LUO Hong-jie, GAO Yan-feng. Preparation and characterization of V_2O_3 micro-crystals via a one-step hydrothermal process [J]. Ceramics International, 2013, 39(7): 7803−7808.

[6] SU D S, SCHLÖGL R. Thermal decomposition of divanadium pentoxide V_2O_5: Towards a nanocrystalline V_2O_3 phase [J]. Catalysis Letters, 2002, 83: 115−119.

[7] YANG Ze-heng, CAI Pei-jun, CHEN Lu-yang, GU Yun-le, SHI Liang, ZHAO Ai-wu, QIAN Yi-tai. A facile route to VN and V_2O_3 nanocrystals from single precursor NH_4VO_3 [J]. Journal of Alloys and Compounds, 2006, 420(1/2): 229−232.

[8] NTULI F, LEWIS A E. Kinetic modelling of nickel powder precipitation by high-pressure hydrogen reduction [J]. Chemical Engineering Science, 2009, 64(9): 2202−2215.

[9] SAARINEN T, LINDFORS L E, FUGLEBERG S. A review of the precipitation of nickel from salt solutions by hydrogen reduction [J]. Hydrometallurgy, 1998, 47(2/3): 309−324.

[10] XU Lei, YAN Qing-zhi, XIA Min, ZHU Ling-xu. Preparation of La_2O_3 doped ultra-fine W powders by hydrothermal-hydrogen reduction process [J]. International Journal of Refractory Metals and Hard Materials, 2013, 36: 238−242.

[11] AGRAWAL A, KUMAR V, PANDEY B D, SAHU K K. A comprehensive review on the hydro metallurgical process for the production of nickel and copper powders by hydrogen reduction [J]. Materials Research Bulletin, 2006, 41(4): 879−892.

[12] LIANG Huan-zhen, TANG Qing, YU Ke-ning, LI Shao-hua, KE Jia-jun. Preparation of metallic silver from Ag_2S slurry by direct hydrogen reduction under hydrothermal conditions [J]. Materials Letters, 2007, 61(4/5): 1020−1022.

[13] ZHANG Guo-bin, ZHANG Yi-min, BAO Shen-xu, HUANG Jing, ZHANG Liu-hong. A novel eco-friendly vanadium precipitation method for hydrothermal hydrogen reduction technology [J]. Minerals, 2017, 7(10): 182.

[14] MARIMUTHU V, DULAC I, KANNOORPATTI K. Significance of Pourbaix diagrams to study the corrosion behaviour of hardfacing alloys based on chromium carbides at 298 K (25 °C) [J]. Journal of Bio- and Tribo-Corrosion, 2016, 2(3): 1−7.

[15] ZHENG Li-cong, LIU Zhan-wei, XIE Ke-qiang, MA Wen-hui, WEI Kui-xian. Thermodynamic research of S−H_2O system in sodium aluminate solution [J]. Key Engineering Materials, 2017, 730: 272−281.

[16] POST K, ROBINS R G. Thermodynamic diagrams for the vanadium−water system at 298.15 K [J]. Electrochimica Acta, 1976, 21(6): 401−405.

[17] ZHOU Xue-jiao, WEI Chang, LI Min-ting, QIU Shuang, LI Xing-bin. Thermodynamics of vanadium–sulfur–water systems at 298 K [J]. Hydrometallurgy, 2011, 106(1/2): 104−112.

[18] CHEN Bian-fang, HUANG Sheng, LIU Biao, GE Qi, XIE Shu-shan, WANG Ming-yu, WANG Xue-wen. Thermodynamic analysis for separation of vanadium and chromium in V(IV)−Cr(III)−H_2O system [J]. Transactions of Nonferrous Metals Society of China, 2018, 28(3): 567−573.

[19] NIE Xian-sheng, CHEN Jing, TAN Qing-lin. Kinetics of iridium reduction by hydrogen in hydrochloric acid solution [J]. Metallurgical Transactions B, 1992, 23(6): 737−745.

[20] ILYAS S, KIM H, RANJAN SRIVASTAVA R. Extraction equilibria of cerium(IV) with Cyanex 923 followed by precipitation kinetics of cerium(III) oxalate from sulfate solution [J]. Separation and Purification Technology, 2021, 254: 117634.

[21] ZHANG Wei-guang, ZHANG Tin-gan, LV Guo-zhi, CAO Xue-jiao, ZHU Hang-yu. Thermodynamic study on the V(V)−P(V)−H_2O system in acidic leaching solution of vanadium-bearing converter slag [J]. Separation and Purification Technology, 2019, 218: 164−172.

[22] YE Guo-hua, HU Yi-bo, TONG Xiong, LU Lu. Extraction of vanadium from direct acid leaching solution of clay vanadium ore using solvent extraction with N235 [J]. Hydrometallurgy, 2018, 177: 27−33.

[23] CHEN Bo, BAO Shen-xu, ZHANG Yi-min. Synergetic strengthening mechanism of ultrasound combined with calcium fluoride towards vanadium extraction from low-grade vanadium-bearing shale [J]. International Journal of Mining Science and Technology, 2021, 31: 1095−1106.

[24] SHOCK E L, SASSANI D C, WILLIS M, SVERJENSKY D A. Inorganic species in geologic fluids: Correlations among standard molal thermodynamic properties of aqueous ions and hydroxide complexes [J]. Geochimica et Cosmogenical Acta, 1997, 61(5): 907−950.

[25] HE Huan-yu, WANG Jie-qi, LI Yang, SONG Ze-yu, SIVAPRASADA M. Thermodynamic analysis of hot water leaching of sulphur from desulphurisation slag by Eh−pH diagrams of the Ca−S−H_2O system [J]. Mineral Processing and Extractive Metallurgy, 2019, 128(3): 161−167.

[26] WANG Jing-peng, ZHANG Yi-min, HUANG Jing, LIU Tao. Kinetic and mechanism study of vanadium acid leaching from black shale using microwave heating method [J]. JOM, 2018, 70(6): 1031−1036.

[27] ROZIER P, RATUSZNA A, GALY J. Comparative structural and electrical studies of V_2O_3 and $V_{2-x}Ni_xO_3$ ($0<x<0.75$) solid solution [J]. Zeitschrift Für Anorganische Und Allgemeine Chemie, 2002, 628(5): 1236−1242.

液相氢还原制备 V_2O_3 的 φ−pH 图和动力学研究

胡艺博[1,2,3,4]，张一敏[1,2,3,4]，薛楠楠[1,2,3,4]，胡鹏程[1,2,3,4]，张刘洪[1,2,3,4]

1. 武汉科技大学 资源与环境工程学院，武汉 430081；
2. 武汉科技大学 国家环境保护矿冶资源利用与污染控制重点实验室，武汉 430081；
3. 钒资源高效利用湖北省协同创新中心，武汉 430081；
4. 武汉科技大学 湖北省页岩钒资源高效清洁利用工程技术研究中心，武汉 430081

摘　要：为了克服 V_2O_3 传统还原焙烧工艺具有的流程长、能耗高、污染大的缺点，采用液相氢还原(SpHR)方法制备 V_2O_3，并对 V−H_2O 体系的 φ−pH 图和沉钒动力学进行分析。V−H_2O 系 φ−pH 图的热力学分析表明：在酸性溶液中，通过液相氢还原制备 V_2O_3 需要较高的温度和钒浓度，以及充足的氢气。动力学研究表明：SpHR 法制备 V_2O_3 的活化能为 38.0679 kJ/mol，表明该过程受界面化学反应和内扩散的混合步骤控制；氢分压(斜率 k=0.05246)对反应速率的影响不如钒浓度(K=1.58872)显著。在 pH=5~6、$c(V_2O_5)$=0.5 mol/L、$p(H_2)$=4 MPa、$m(PdCl_2)$=10 mg、T=250 °C 及 t=2.5 h 的条件下，获得纯度为 99.59%和沉钒率为 99.83%的 V_2O_3 晶体。

关键词：V_2O_3；液相氢还原；φ−pH 图；动力学

(Edited by Xiang-qun LI)